Magnetic Color Symmetry of Lattice Rotations in a Diamagnetic Material

S. Denev,[1] A. Kumar,[1] M. D. Biegalski,[1] H. W. Jang,[2] C. M. Folkman,[2] A. Vasudevarao,[1] Y. Han,[3] I. M. Reaney,[3]
S. Trolier-McKinstry,[1] C.-B. Eom,[2] D. G. Schlom,[1] and V. Gopalan[1]

[1]*Department of Materials Science and Engineering, Pennsylvania State University, University Park, Pennsylvania 16802, USA*
[2]*Department of Materials Science and Engineering, University of Wisconsin–Madison, Madison, Wisconsin 53706, USA*
[3]*Department of Engineering Materials, The University of Sheffield, Sheffield S1 3JD, United Kingdom*

Oxygen octahedral rotations are the most common phase transitions in perovskite crystal structures. Here we show that the color symmetry of such pure elastic distortions is isomorphic to magnetic point groups, which allows their probing through distinguishing polar versus magnetic symmetry. We demonstrate this isomorphism using nonlinear optical probing of the octahedral rotational transition in a compressively strained $SrTiO_3$ thin film that exhibits ferroelectric ($4mm$) and antiferrodistortive ($4'mm'$) phases evolving through independent phase transitions. The approach has broader applicability for probing materials with lattice rotations that can be mapped to color groups.

The oxygen octahedron is a basic structural unit in perovskite and related complex oxides (ABO_3, where A and B are cations) that span a wide range in properties including superconducting, semiconducting, insulating, magnetic, ferroelectric, and multiferroic phenomena. Octahedral rotational transitions, involving rotations of the octahedral units BO_6, are by far the most common phase transitions to occur in perovskites [1,2]. In a large number of these materials, the rotation of the octahedral units is intimately related to the stability of the perovskite phase through reduction of the volume of the interstices and improving the structural stability. Goldschmidt [3] demonstrated that for an ABO_3 ferroelectric, the perovskite phase will form if $t = (R_A + R_O)/\sqrt{2}(R_B + R_O)$ is close to 1, where R_A, R_B, and R_O are the radii of the A- and B-site cations and the O ion, respectively. Reaney *et al.* [4] showed that at room temperature, perovskites with $0.985 < t < 1.06$ are expected to have untilted octahedra; perovskites with $0.964 < t < 0.985$ usually contain antiphase octahedral rotations, and perovskites with $t < 0.964$ are expected to show in-phase and antiphase octahedral rotations. As t continues to decrease, the stability of the perovskite phase decreases and eventually other structures predominate. In addition to stability, the octahedral rotation is often connected closely with anomalies in the physical properties. For example, both the intrinsic and extrinsic contributions to the piezoelectric properties of $Pb(Zr_{1-x}, Ti_x)O_3$ are a function of tilting [5,6], the temperature dependence of the dielectric properties of microwave dielectrics [4,7], as well as the spin canting in the multiferroic $BiFeO_3$ [8] are closely connected to octahedral rotations.

The traditional methods for studying octahedral rotations are primarily neutron, x-ray, and electron diffraction. It is difficult, however, to detect such distortions with very weak diffraction signatures in very thin layers due to small volume, weak oxygen scattering, and substrate interference. However, we show that the color symmetry of these distortions are isomorphic to magnetic point groups, which allows nonlinear optical probing of crystallographic versus magnetic symmetries. Conventionally, these rotation phases are described in Glazer notation [1]. For example, $SrTiO_3$ exhibits an antiferrodistortive (AFD) phenomena involving rotation of adjacent octahedra in opposite senses (see Fig. 1) only about the [001] surface normal direction in compressively strained thin films [9]. The point group symmetry of this AFD phase in compressively strained thin films is conventionally expressed in Glazer notation as $4mm$ ($a^0a^0c^-$), where a^0 refers to zero lattice rotation about the in-plane [100] and [010] directions, and c^- refers to antidistortive rotation about the [001] direction, of the adjacent oxygen octahedra (001) planes. This notation, however, masks the true color symmetry of these lattice distortions. The same structure can also be described by the color point group $4'mm'$, as seen in Fig. 1. Here $1'$ indicates an antisymmetric operator that results in a reversal of the sense of all rigid octahedral rotations about their rotation axes. From a symmetry perspective, this operator is similar to a time-reversal operator, which is also antisymmetric and reverses the spin or magnetic moment by reversing the sense of a current loop. Birss [10], for example, discusses similar generalization of time reversal to any antisymmetric operation that changes the sign of an attribute. Hence, for all practical purposes, the antiferrodistortive group $4'mm'$ is isomorphic to the magnetic point group $4'mm'$, which is the symmetry of a C-type antiferromagnet. Such an isomorphic mapping can be made, in general, between all antidistortive elastic point groups and magnetic point groups. There are deeper implications for such isomorphic mapping of magnetic point groups to pure structural distortions, even rigid. The 2-color symmetry $4'mm'$ immediately implies the presence of certain tensor properties that are distinct from their polar counterpart expected from the $4mm$ point group. Probing these properties can thus
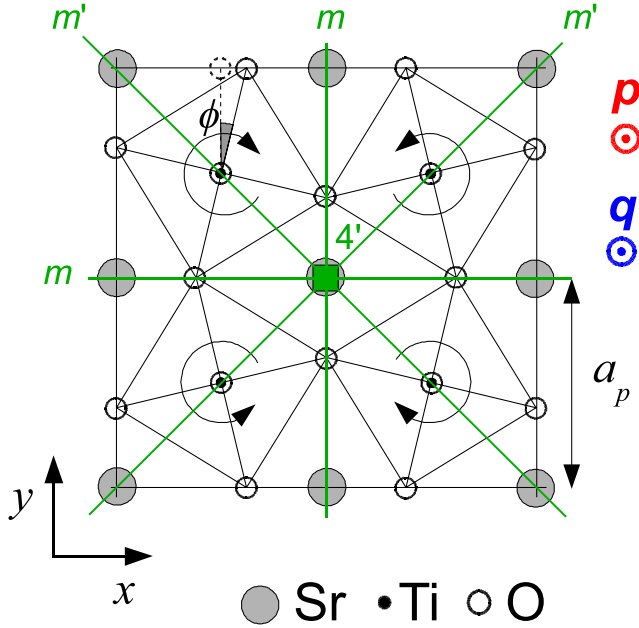
FIG. 1 (color online).   AFD transition in SrTiO₃ manifested by
rotation of the neighboring oxygen octahedra in opposite direc-
tion by angle ϕ resulting in an enlarged unit cell with lattice
parameters $\sqrt{2}a_p \times \sqrt{2}a_p \times 2a_p$ where a_p is the pseudocubic
lattice parameter. The ferroelectric polarization vector **p** and the
AFD vector **q** are pointing out of the plane. Also shown in green
are the resulting symmetry elements of the $4'mm'$ point group.

allow for detecting the unique signature of such octahedral
lattice rotations distinct from the ferroelectric polarization.
Such detection is shown in this Letter where optical second
harmonic generation is used to probe second order optical
polarizability (third rank tensor) to distinguish ferroelectric
(FE) ($4mm$) and AFD ($4'mm'$) phases in strained SrTiO₃
through a broad overlapping phase transitions where both
these phases coevolve with temperature. Other second
harmonic generation (SHG) studies have distinguished
ferroelectric and magnetic order parameters in magnetic
and multiferroic materials [11], based on their polar versus
magnetic symmetries, respectively. In our study, we probe
a diamagnetic material such as SrTiO₃, which has pure
lattice distortions whose symmetry, nonetheless, resembles
a magnetic point group.

We study the phase transitions in a 500 Å thick, fully
commensurate SrTiO₃ film grown on a NdGaO₃ (110)
substrate by pulsed laser deposition. The in-plane lattice
parameters of the film were found to be $a = 3.859 \pm
0.001$ Å and the out-of-plane spacing was $c =
3.968 \pm 0.001$ Å. This shows a nearly commensurate
film with the in-plane pseudocubic lattice parameters of
the NdGaO₃ substrate being $\sqrt{a^2 + b^2}/2 = 3.864 \pm
0.001$ Å along the $[1\bar{1}0]$ direction and $c/2 = 3.839 \pm
0.001$ Å along the [001] direction [12]. This corresponds
to an in-plane biaxial compressive strain of 1.18%. Theory
predicts [13] that between 180 K and 420 K, the film will

assume a noncentrosymmetric tetragonal ferroelectric state
with $4mm$ symmetry and polarization **p** along the [001]
direction (out of the growth plane; also labeled as z or
3-axis) [14]. In addition, the AFD transition is predicted to
occur below 180–200 K. This transition is characterized
by an order parameter **q** pointing out of the plane in the z
(or 3) direction, and proportional to the rotation angle ϕ of
the oxygen octahedra (see Fig. 1), given by $q = (a_p/2) \times
\tan\phi$. Yamada *et al.* [15] and Vasudevarao *et al.* [9] have
previously studied strained SrTiO₃ films. No attempt, how-
ever, to study the symmetry of the ferroelastic phase was
made.

In our study, we employ optical second harmonic gen-
eration. This technique involves the conversion of light
with optical frequency ω and electric field E^ω to light
with frequency 2ω and electric field $E^{2\omega}$ through the
generation of nonlinear polarization in the material, $P_i^{2\omega} \propto
d_{ijk}E_j^\omega E_k^\omega$, where d_{ijk} is the polar nonlinear optical tensor
that couples to polar order parameter **p**. The equivalent
axial tensor Q_{ijk} that couples to axial order parameter **q** is
involved in the interactions of type $P_i^{2\omega} \propto Q_{ijk}E_j^\omega H_k^\omega$, or
$M_i^{2\omega} \propto Q_{ijk}E_j^\omega E_k^\omega$ to the lowest order. Though an axial
(polar) order parameter does not couple exclusively to an
axial (polar) tensor property, these are the tensors that we
are interested in probing in order to find symmetry dis-
tinctions between the AFD and FE phases. We call this
property the roto-SHG effect, in analogy with the
magnetic-SHG effect. The fundamental light used for the
experiments was generated by a mode-locked Ti:sapphire
laser tuned at 800 nm with 80 fs pulses and an 80 MHz
repetition rate. It was chopped at a frequency of 800 Hz to
allow lock-in detection.

We used a transmission geometry with the film facing
the incident light and the sample placed inside an optical
cryostat allowing the temperature to be varied between 4 K
and 350 K. Since light in normal incidence ($\varphi_i = 0°$)
along the z axis does not generate any SHG for $4mm$
symmetry, our sample was tilted by an angle $\varphi_i = 45°$
with respect to the input laser (inset of Fig. 2) with x–z as
the incidence plane. No SHG was observed from the bare
NdGaO₃ substrate. The intensity $I^{2\omega}$ of the output SHG
signal at 400 nm was detected along either the s or p
polarization directions with a photomultiplier tube while
the angle of polarization of the incident light with respect
to the incident plane was varied continuously using a $\lambda/2$
wave plate. The resulting polar plots at room temperature
are shown in Figs. 2(a) and 2(b) for the p and s polar-
izations, respectively.

The nonzero coefficients for the $4mm$ polar tensor (FE
phase) are $d_{15} = d_{24}$, $d_{31} = d_{32}$, and d_{33}, where the usual
tensor abbreviation of the j and k subscripts are performed.
On the other hand, the nonzero coefficients for $4'mm'$ axial
tensor Q_{ijk} are only $Q_{14} = Q_{25}$ and Q_{36}. These coefficients
are different and complementary, and hence can help dis-
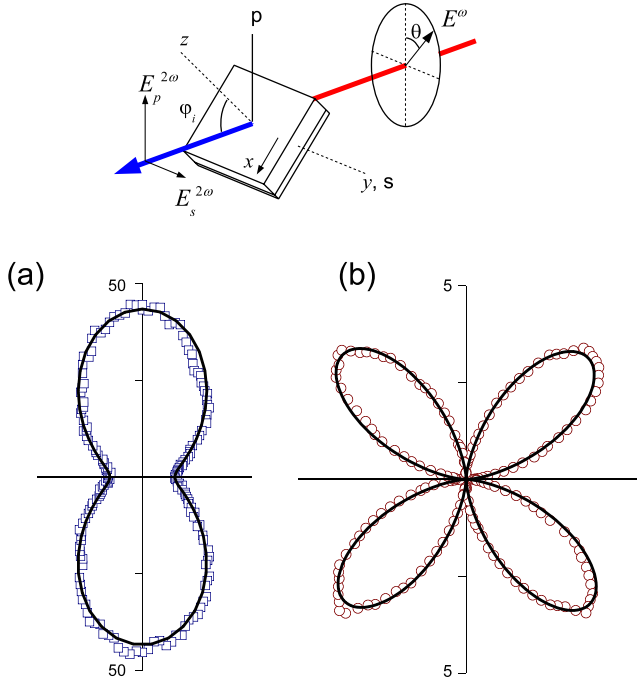tinguish the FE from the AFD phases. If we assume that

FIG. 2 (color online). Polar plots for p (a) and s (b) output polarizations at room temperature. Solid lines show fits to Eq. (1). Inset: schematic of the experimental setup.

both AFD and FE phases give rise to SHG signals that interfere, then the resultant SHG intensity for the p and s polarizations in our geometry can be generally derived as

$$I_p(\theta) = (A\cos^2\theta + B\sin^2\theta + D\sin2\theta)^2$$
$$I_s(\theta) = (C\sin2\theta + E\cos^2\theta)^2, \tag{1}$$

where

$$A = \sqrt{I_0}t_p(\tilde{f}_x^T f_x f_z d_{15}\sin2\varphi_i + \tilde{f}_z^T f_x^2 d_{31}\cos^2\varphi_i$$
$$+ \tilde{f}_z^T f_z^2 d_{33}\sin^2\varphi_i)$$
$$B = \sqrt{I_0}t_p\tilde{f}_z^T f_y^2 d_{31} \qquad C = \sqrt{I_0}t_s\tilde{f}_y^T f_y f_z d_{15}\sin\varphi_i \tag{2}$$
$$D = \sqrt{I_0}t_p(\tilde{f}_x^T f_y f_z Q_{14}\sin\varphi_i - \tilde{f}_z^T f_x f_y Q_{36}\cos\varphi_i)$$
$$E = \sqrt{I_0}t_s\tilde{f}_y^T f_x f_z Q_{14}\sin2\varphi_i.$$

The coefficients A, B, C, D, and E are functions only of the incident angle φ_i, the coefficients d_{ij} and Q_{ij} of the film, and the indices of refraction of the film and substrate. The terms f_i ($i = x$, y, z) represent the linear Fresnel coefficients for transmission of the incident fundamental light through the air-film interface while the terms $\tilde{f}_i^T$ are the nonlinear Fresnel coefficients for the generation of light of frequency 2ω in the film [16]. I_0 is the intensity of the incident light and $t_{p,s}$ are the Fresnel coefficients for transmission of light through the substrate-air interface. Further, in Eq. (1), the polar and the AFD components are symmetry distinct (but optically interfere): the polar signal

arising from $4mm$ symmetry of the FE phase is given by the coefficients A, B, and C, and the AFD signal arising from the $4'mm'$ is given by D and E. We can thus calculate the relative contribution of the AFD component to the overall SHG signal as

$$\frac{I_p^{AFD}}{I_p^{FE+AFD}} = \frac{D^2}{(A/2 + B/2 + D)^2}, \tag{3}$$

where we have chosen the angle of input polarization $\theta = 45°$ to maximize the contribution of the AFD component. The AFD contribution as a function of temperature is shown in Fig. 3(b). In order to highlight the transitions, we also plot an effective nonlinear optical coefficient (in normalized units) as $\bar{d}_{eff} = A^2/B^2$. This coefficient depends only on the nonlinear optical coefficients, arising from the dominant polar contributions, and the linear and nonlinear Fresnel coefficients. Therefore any change in $\bar{d}_{eff}$ will be indicative of changes in the material properties of the film. Plotting $\bar{d}_{eff}$ vs temperature reveals three distinct regions in the film with transitions at ~150 K, 250 K, and 400 K, as shown in Fig. 3(b). Note that the dominant SHG signal at all temperatures was the polar FE contribution arising from $4mm$ symmetry, with the maximum fraction of AFD signal arising from the $4'mm'$ phase only ~3% of the polar signal. While a direct detection of this AFD signal is challenging, the interference of the AFD signal with the polar signal results in a slight rotation of the SHG polar plots in Fig. 2. In particular, the symmetry considerations from Eq. (1) are such that angles θ where the AFD signal (arising from terms D, E) is maximum also exactly coincide with where the FE signal (arising from A, B, C) is minimum, and vice versa. Since these angular minima in
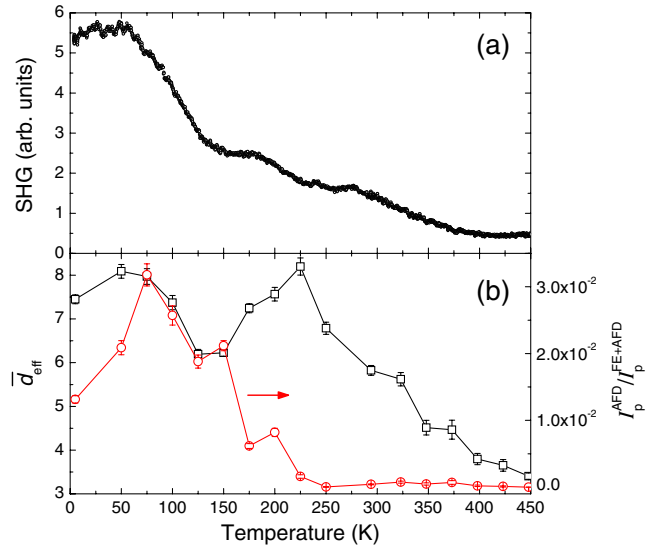

FIG. 3 (color online). (a) Temperature dependence of the second harmonic signal. (b) Temperature dependence of the effective nonlinear coefficient $\bar{d}_{eff}$ and the AFD contribution to the overall SHG signal.

the experimental polar plots of SHG are very precise, and carefully calibrated to the film and substrate crystallographic axes, any angular rotation of these minima due to a small AFD signal was sensitively detected and extracted from numerical fits to experiments.

This analysis allows us to present a possible picture of the transitions taking place in the film. Upon cooling, the FE transition occurs at ~ 400 K where the SHG signal [Fig. 3(a)] and the $\bar{d}_{\text{eff}}$ begin to appear. The AFD transition begins at $T_{\text{AFD}} \sim 250$ K, with the relative SHG component of the AFD increasing with cooling. This coincides with an anomaly in $\bar{d}_{\text{eff}}$. By ~ 75–150 K, both FE and AFD transitions are complete, and film is multiferroic below this transition.

The clear separation of the FE and AFD phase transitions in the film excludes the possibility that the axial SHG signal that appears only at the AFD transitions could instead arise simply from the polar $4mm$ phase through multipole expansion terms in the induced nonlinear electric or magnetic polarizations created by laser light. Such a contribution, if present, could arise only from induced diamagnetic spins in $SrTiO_3$ by the magnetic field of light, coupling to a fourth ranked polar susceptibility tensor. However, such contributions are too small to measure within our measurement sensitivity, as seen from the negligible AFD contribution across the ferroelectric transition. As further evidence, we also studied a 1% compressively strained $BaTiO_3$ film on $GdScO_3$ substrate, which is identical in symmetry with the $SrTiO_3$ film, and has enhanced ferroelectric transition at ~ 700 K. (See Ref. [17] for more details on the SHG study of this film system, which we have revisited for this study.) However, and this is key, this film does not have any AFD phase, predicted or observed. Indeed, axial SHG signal was absent across the FE transition in this film system, as expected. Finally, we studied a partially relaxed $SrTiO_3$ film on the $NdGaO_3$ substrate with a 0.85%–0.97% compressive strain. In this case, an AFD transition at ~ 250 K that precedes a FE transition at 200 K was observed by the same technique, in agreement with theory predictions. Thus, based on these three strained film systems studied here, all with $4mm$ polar phase, axial SHG signals are observed only when an AFD phase is present and at the temperatures it is predicted, and is absent otherwise. We note that a direct and independent measurement of the Q_{36} coefficient would further confirm the $4'mm'$ symmetry of the AFD phase. This was, however, not possible in our thin film study since Q_{36} and Q_{14} occur together for any non-normal sample tilt as seen from Eq. (3). In normal incidence, no SHG is expected from FE or AFD phases.

In conclusion, we show that the symmetry of pure elastic lattice in the antiferrodistortive phase in $SrTiO_3$ is isomorphic to magnetic point group $4'mm'$. This symmetry mapping has real implications, as shown here in probing the lattice rotation transition using optical SHG that distinguishes polar versus magnetic symmetries. More generally, such symmetry mapping can apply to all materials with lattice antidistortions with color groups that are isomorphic to magnetic point groups, whether the material itself has magnetism or not. Further, one can also use a variety of other higher-order tensor properties besides SHG to probe the antidistortions isomorphic with magnetic symmetry. For example, in analogy with magnetoelectric and magnetostrictive effects, one can imagine symmetry allowed rotoelectric and rotostrictive effects.

[1] A. M. Glazer, Acta Cryst. B **28**, 3384 (1972).
[2] A. M. Glazer, Acta Cryst. A **31**, 756 (1975).
[3] V. M. Goldschmidt, Fortschr. Mineral. **15**, 73 (1931).
[4] I. M. Reaney, E. L. Colla, and N. Setter, Jpn. J. Appl. Phys. **33**, 3984 (1994).
[5] H. Zheng, I. M. Reaney, W. E. Lee, N. Jones, and H. Thomas, J. Am. Ceram. Soc. **85**, 2337 (2002).
[6] R. Eitel and C. A. Randall, Phys. Rev. B **75**, 094106 (2007).
[7] M. B. Telli, S. S. N. Bharadwaja, M. D. Biegalski, and S. Trolier-McKinstry, Appl. Phys. Lett. **89**, 252907 (2006).
[8] C. Ederer and N. A. Spaldin, Phys. Rev. B **71**, 060401(R) (2005).
[9] A. Vasudevarao *et al.*, Phys. Rev. Lett. **97**, 257602 (2006).
[10] R. Birss, *Symmetry and Magnetism* (North-Holland, Amsterdam 1964), Chap. 6.
[11] M. Fiebig, Th. Lottermoser, D. Fröhlich, A. V. Goltsev, and R. V. Pisarev, Nature (London) **419**, 818 (2002).
[12] M. Sasaura, S. Miyazawa, and M. Mukaida, J. Appl. Phys. **68**, 3643 (1990).
[13] Y. L. Li *et al.*, Phys. Rev. B **73**, 184112 (2006).
[14] A. Antons, J. B. Neaton, K. M. Rabe, and D. Vanderbilt, Phys. Rev. B **71**, 024102 (2005).
[15] T. Yamada *et al.*, Phys. Rev. Lett. **96**, 157602 (2006).
[16] B. Dick, A. Gierulski, G. Marowsky, and G. A. Reider, Appl. Phys. B **38**, 107 (1985).
[17] K. J. Choi *et al.*, Science **306**, 1005 (2004).